



RESEARCH ARTICLE

Histone demethylase complexes KDM3A and KDM3B cooperate with OCT4/SOX2 to define a pluripotency gene regulatory network

Zhenshuo Zhu¹  | Xiaolong Wu¹ | Qun Li² | Juqing Zhang¹ | Shuai Yu¹ | Qiaoyan Shen¹ | Zhe Zhou¹ | Qin Pan¹ | Wei Yue¹ | Dezhe Qin¹ | Ying Zhang¹ | Wenxu Zhao¹ | Rui Zhang¹ | Sha Peng¹ | Na Li¹ | Shiqiang Zhang¹ | Anmin Lei¹ | Yi-Liang Miao³ | Zhonghua Liu⁴ | Xingqi Chen⁵ | Huayan Wang¹ | Mingzhi Liao² | Jinlian Hua¹ 

¹College of Veterinary Medicine, Shaanxi Centre of Stem Cells Engineering & Technology, Northwest A&F University, Yangling, China

²College of Life Science, Northwest A&F University, Yangling, China

³Institute of Stem Cell and Regenerative Biology, College of Animal Science and Veterinary Medicine, Huazhong Agricultural University, Wuhan, China

⁴Key Laboratory of Animal Cellular and Genetic Engineering of Heilongjiang Province, College of Life Science, North-East Agricultural University, Harbin, China

⁵Department of Cell and Molecular Biology, Karolinska Institutet, Solna, Sweden

Correspondence

Mingzhi Liao, College of Life Science, Northwest A&F University, Yangling, Shaanxi, 712100, China.
Email: liaomz@nwsuaf.edu.cn

Jinlian Hua, College of Veterinary Medicine, Northwest A&F University, Shaanxi Centre of Stem Cells Engineering & Technology, No. 3rd, Taicheng Road, Yangling, Shaanxi, 712100, China.
Email: jinlianhua@nwsuaf.edu.cn

Funding information

This work was supported by grants from Program of National Natural Science Foundation of China (32072806, 62072377); The National Key Research and Development Program of China Stem Cell and Translational Research (Grant No.2016YFA0100203), Program of Shaanxi Province Science and Technology Innovation Team (2019TD-036), the China

Abstract

The pluripotency gene regulatory network of porcine induced pluripotent stem cells (piPSCs), especially in epigenetics, remains elusive. To determine the biological function of epigenetics, we cultured piPSCs in different culture conditions. We found that activation of pluripotent gene- and pluripotency-related pathways requires the erasure of H3K9 methylation modification which was further influenced by mouse embryonic fibroblast (MEF) served feeder. By dissecting the dynamic change of H3K9 methylation during loss of pluripotency, we demonstrated that the H3K9 demethylases KDM3A and KDM3B regulated global H3K9me2/me3 level and that their co-depletion led to the collapse of the pluripotency gene regulatory network. Immunoprecipitation-mass spectrometry (IP-MS) provided evidence that KDM3A and KDM3B formed a complex to perform H3K9 demethylation. The genome-wide regulation analysis revealed that OCT4 (O) and SOX2 (S), the core pluripotency transcriptional activators, maintained the pluripotent state of piPSCs depending on the H3K9 hypomethylation. Further investigation revealed that O/S cooperating with histone demethylase complex containing KDM3A and KDM3B promoted pluripotency

Abbreviations: DEGs, differentially expressed genes; DOX, doxycycline; ESCs, embryonic stem cells; IP-MS, immunoprecipitation-mass spectrometry; iPSCs, induced pluripotent stem cells; MEF, mouse embryonic fibroblast; mESCs, mouse embryonic stem cells; pESLCs, porcine embryonic stem cell-like cells; piPSCs, porcine induced pluripotent stem cells; pPSCs, porcine pluripotent stem cells; TetO, tetracycline operator.

Zhenshuo Zhu, Xiaolong Wu and Qun Li equally contributed to this manuscript.

Postdoctoral Science Foundation National Natural Science Foundation of China (32002246), Fundamental research funds for the central Universities, NWSUAF (Z1090219146, Z102022004).

genes expression to maintain the pluripotent state of piPSCs. Together, these data offer a unique insight into the epigenetic pluripotency network of piPSCs.

KEYWORDS

H3K9 methylation, histone demethylase complexes, KDM3A/3B, pluripotency

1 | INTRODUCTION

The acquisition of pluripotency depends on the reconstruction of the epigenetic modification during reprogramming. Recent studies have shown that OCT4, SOX2, and KLF4 cooperating with epigenetic modifiers mediated the gradually silencing of differentiation genes and activating of pluripotency genes simultaneously during reprogramming.^{1,2} Of note, global H3K9 methylation is erased in the later stages of the reprogramming with the activation of pluripotency network.^{3,4} Therefore, the establishment of pluripotent epigenetic regulation network based on histone modification should be the kernel for maintaining the pluripotent state of induced pluripotent stem cells (iPSCs).⁴

As an epigenetic modification associated with transcriptionally repressing, H3K9 methylation is a major hindrance during somatic cell reprogramming into iPSCs.^{3,4} Loss of H3K9 methylation significantly increases the expression of endogenous pluripotent genes and contributes to the transition of pre-iPSCs into iPSCs.^{3,5} Previous studies also demonstrated that the increase of H3K9 methylation causes the loss of pluripotency in mouse embryonic stem cells (mESCs).⁶⁻⁸ However, the molecular mechanism underlying H3K9 hypomethylation in pluripotent gene regions remains unclear in pluripotent stem cells. The KDM3 family, which includes KDM3A and KDM3B, function as epigenetic activators to demethylate intrinsic H3K9 methylation modification.^{9,10} Additionally, KDM3A has been found to play a critical role in a wide range of biological process like embryo development,⁸ pluripotency maintenance,⁶ carcinogenesis,^{11,12} cell senescence,¹³ sex differentiation,¹⁴ and spermatogenesis.^{15,16} At the same time, KDM3B exhibits similar functions like KDM3A, such as pluripotency maintenance,^{5,7} carcinogenesis,¹⁷ and spermatogenesis.¹⁸ However, the elaborate mechanism of KDM3A and KDM3B in pluripotency maintenance and their functional redundancy in H3K9 demethylation remain unclear.

Pig is an ideal model for human medical research due to its close similarity with human in genetic, anatomical, and physiological condition.^{19,20} Research on porcine PSCs contributes to promising value in the biomedical field,²⁰ though most published porcine PSCs, including ESCs and iPSCs, cannot meet with the stringent criteria for pluripotency identity. We hypothesized the unsound pluripotency gene regulatory network of piPSCs, especially in epigenetics, would be the major obstacle for us to obtain bona fide PSCs in vitro. To solve this issue,

the present study used piPSCs generated by tetracycline operator (TetO)-inducible system²¹ to delineate the mechanism of H3K9 demethylation in piPSCs. Here, we found that KDM3A/KDM3B-mediated H3K9 demethylation plays a critical role in pluripotency maintenance of piPSCs. Moreover, the rescue experiment suggested that not all exogenous genes were required and only O/S were essential for the pluripotency maintenance of piPSCs. By performing genome-wide analysis of H3K9me2/me3 modification and O/S occupancy enrichment by ChIP-seq, as well as KDM3A and KDM3B interactome analysis by IP-MS, we thus reveal the novel pluripotency regulation pathway, in which SOX2/OCT4 recruit chromatin remodeling proteins KDM3A/KDM3B to form a transcriptional complex to drive the pluripotency gene regulatory network.

2 | MATERIAL AND METHODS

2.1 | Cell culture

Porcine iPSCs was cultured on feeder (MEF, mouse embryonic fibroblasts) and maintained in LB2i medium, consisting of DMEM (Hyclone, USA) supplemented with 15% FBS (VISTECH, New Zealand), 0.1 mM NEAA (Gibco, USA), 1 mM L-glutaMAX (Gibco, USA), 10 ng/mL LIF (Sino Biological, 14890 -HNAE), 10 ng/mL bFGF (Sino Biological, 10014-HNAE), 0.1 mM β -mercaptoethanol (Sigma Aldrich, M3148, USA), 3 μ M CHIR99021 (MCE, HY-10182), 2 μ M SB431542 (Selleck, S1067), 4 μ g/mL doxycycline (Sigma Aldrich, D9891), 100 units/mL penicillin, and 100 μ g/mL streptomycin. piPSCs were passaged using TrypLE Select (Invitrogen, USA) into a single cell at 2×10^4 cells per 12-well plate every 5-6 days. Differentiation was performed in differentiation medium: DMEM (Hyclone, USA) supplemented with 15% FBS, 0.1 mM NEAA, 1 mM L-glutaMAX, 0.1 mM β -mercaptoethanol, 100 units/mL penicillin, and 100 μ g/mL streptomycin. HEK293T and MEFs were cultured in DMEM supplemented with 10% FBS and 100 units/mL penicillin, 100 μ g/mL streptomycin.^{21,22}

2.2 | Plasmids and cloning

All lentivirus backbone vectors were derived from pCDH-CMV-MCS-EF1-GreenPuro (CD513B-1, SBI, Mountain

View, CA, USA) by Seamless Cloning and Assembly Kit (Novoprotein, China). The following vectors used in this study were constructed using the same strategy and its information is shown in Table S1.

2.2.1 | shRNA vectors

shRNAs were designed using the online shRNA design tool from Invitrogen (<http://rnaidesigner.thermofisher.com/rnaexpress/setOption.do?designOption=shrna&pid=5230999276329139407/>) with default parameters. And the potential off-target effects were filtered out using BLAST against the porcine genome.

Sense and antisense oligonucleotides of the shRNA duplex were synthesized and cloned into an in-house designed pCDH-U6-MCS-EF1-GFP-T2A-PURO or pCDH-U6-MCS-EF1-GFP-T2A-mCherry Lentivector. All shRNAs were tested for each gene in piPSCs and knockdown efficiencies of 70% or more were used in this study. The vector and sequence information of shRNAs used in this study is shown in Tables S1 and S2.

2.2.2 | Overexpression vectors

The p-O/S/K/M/L(*OCT4/SOX2/KLF4/c-MYC/LIN28A*) gene were PCR-amplified from porcine blastocysts and subcloned into an in-house pCDH-EF1-MCS-T2A-PURO vectors. The 3×FLAG-OCT4, 3×FLAG-SOX2, 3×FLAG-KDM3A, and 3×FLAG-KDM3B were generated by PCR and subcloned in pCDH-TetO-3XFLAG-MCS-T2A-PURO. The Rosa26-EF1α-3×FLAG-OCT4, and Rosa26-EF1α-OCT4-P2A-SOX2 were generated by PCR and subcloned in Rosa26-EF1α-MCS-T2A-PURO. Coding regions of all overexpression vectors were verified by sequencing. Subsequently, these overexpression vectors were transfected into HEK293T cell and identified by Western blot. The vector information of these genes used in this study is shown in Table S1.

2.2.3 | BiFC vectors

The *OCT4/SOX2/KDM3A/KDM3B/WNT2* gene were generated by PCR and subcloned in pBiFC-VC155 and pBiFC-VN173. Coding regions of all overexpression vectors were verified by sequencing. The vector information of these genes used in this study is shown in Table S1.

2.2.4 | Luciferase vectors

To verify the ChIP-seq of OCT4 and SOX2, the porcine target gene promoter and enhancer were amplified by PCR from

total genomic DNA extracted from piPSCs and subcloned into an in-house PGL3-basic vector (Promega, E1751) by Seamless Cloning. The detailed information of these Luciferase vectors is shown in Table S1.

2.3 | Lentivirus packaging and transduction

HEK293T cells were seeded onto a six-well plate and grown to 70%-80% confluence. Then the lentivirus backbone and package vector (pVSV-G and psPAX2) were transfected into HEK293T cells using PEI (polyethyleneimine, sigma). For transfection of per well, 1 μg pVSV-G, 1 μg psPAX2, and 2 μg lentivirus backbone vector were diluted in 200 μL optiMEM and vortexed. A quantity of 12 μL PEI (1 mg/mL) was added to the plasmid mix, vortexed, incubated for 15 minutes at room temperature and then added to cells. After 12 hours, the medium was replaced with fresh medium added lipid and cells were maintained for 48-72 hours. Lentivirus (culture supernate) was collected, filtered through 0.45 μm filter to remove debris. For the lentiviral transduction, 2×10^4 cells were plated on MEF-coated 12 well plate per well and allowed to attach overnight. Virus and fresh media were added at a ratio of 1:1 supplemented with 4 μg/mL polybrene into this well. The cells were incubated with mixed media overnight, washed with PBS and replaced with fresh medium. After 1 week of culture, stably infected colonies were selected with puromycin (10 μg/mL) for 24 hours, and viral titer was calculated by counting the GFP-positive colonies.

2.4 | AP staining

Cells were fixed with 4% paraformaldehyde in PBS (pH 7.4) for 15 minutes at room temperature, washed twice using ice-cold PBS and developed with AST Fast Red TR and α-Naphthol AS-MX Phosphate (Sigma Aldrich) according to the manufacturer's instructions. Then the cells were incubated with the mixture (1.0 mg/mL Fast Red TR, 0.4 mg/mL Naphthol AS-MX in 0.1 M Tris-HCL Buffer) at room temperature. After 20 minutes, the AP-positive iPS colonies showed in red color. The images were collected by a Nikon phase contrast microscope.

2.5 | RNA extraction, reverse transcription, and quantitative real-time PCR

Total RNA was extracted by RNAiso Plus (Takara, 9109) and purified with the guanidine isothiocyanate-phenol chloroform. Reverse transcription was performed using Fast Quant RT Kit (TIANGEN, KR106). Fluorescence quantitative PCR

analyses of all samples were performed using a Bio-Rad CFX96 and SYBR green master mix (TIANGEN, FP215). Semi-quantitative PCR reactions were performed for 30 cycles by 2×TSINGKE Master Mix (TSINGKE, TSE004). The primer information used in this study is provided in Table S3. The expression of target gene was normalized against transfection of control vector. Data of Q-PCR are calculated by Bio-Rad software CFX3.1 and derived from three independent experiments.

2.6 | Western blot

The cells were digested by TrypLE Select and then transferred immediately to a 1.5-mL tube on ice. The cell suspension was then centrifuged at 5000g for 3 minutes and supernatant was discarded. The cell sediment was lysed by RIPA buffer (Beyotime, P0013B) for 30 minutes on ice, added to 5× SDS-PAGE loading buffer (GENSHARE G, JC-PE007), and heated at 100°C for 5 minutes, then loaded onto 8%-12% SDS-PAGE gel. The SDS-PAGE gels were run at 100V for 1.5 hours and transferred to a PVDF membrane by semidry electrophoretic transfer (Bio-Rad) for 45 minutes at 15 V. The transferred membrane was blocked with 8% skim milk at room temperature for 2 hours, and then incubated with the primary antibody in TBS-T buffer (20 mM Tris/HCl pH 8.0, 150 mM NaCl, 0.05% Tween 20) at 4°C overnight. After washing three times with TBS-T buffer, the blot was incubated with secondary antibody at 37°C for 1 hour, then washed three times. Enhanced chemiluminescent substrate (Biodragon, BF06053-500) was used to detect the HRP signal and the western blot images were collected using the Chemiluminescent Imaging System (ZY058176, Tanon-4200, China). The information of antibodies used in this study was listed in Table S4.

2.7 | Immunofluorescence staining

The cells were fixed with 4% paraformaldehyde in PBS (pH 7.4) for 15 minutes at room temperature. Fixed cells were washed twice using ice-cold PBS, permeabilized with 0.1% Triton X-100 in PBS for 10 minutes, and subsequently blocked for 2 hours at room temperature in PBS containing 5% FBS. The cells were incubated with blocking buffer containing primary antibodies at 4°C overnight. The secondary antibodies were diluted in a blocking buffer and incubated at 37°C for 1 hour. After washing with PBS for three times, the nuclei were stained by 10 µg/mL Hoechst 33342 for 8 minutes. Finally, the images were collected by an EVOS fluorescence microscope. The information of antibodies used in this study was listed in Table S4.

2.8 | Chromatin immunoprecipitation and ChIP-seq

2.8.1 | ChIP assay

The 1×10^7 cells were cross-linked with 1% formaldehyde for 10 minutes at room temperature, then added to 125 mM Glycine to neutralize the formaldehyde. The cross-linked cells were washed three times using ice-cold PBS, subsequently scraped off and transferred to a 15 mL centrifuge tube. The cell suspension was spun down for 5 minutes at 2000g and the supernatant was completely removed. The sediments were lysed by Nuclear Lysis Buffer to obtain chromatin extracts, that were treated with ultrasound to obtain DNA fragments with an average size of 200-500 bp. The complexes of target proteins and DNA fragments are immunoprecipitated by specific antibodies and protein A/G magnetic beads. The information of antibodies used in this study were listed in Table S4.

2.8.2 | ChIP-seq and data analysis

The DNA fragments of IP and Input were used for stranded DNA library preparation. Then the library was detected by agarose electrophoresis, quantified using Qubit 2.0 and sequenced on Illumina HiSeq2500 PE150. Raw sequencing data was first filtered by Trimmomatic²³ (version 0.36), low-quality reads were discarded and the reads contaminated with adaptor sequences were trimmed. The clean reads were mapped to the reference genome of *Sus scrofa* from GCF_000003025.6 (ftp://ftp.ncbi.nlm.nih.gov/genomes/all/GCF/000/003/025/GCF_000003025.6_Sscrofa11.1/GCF_000003025.6_Sscrofa11.1_genomic.fna.gz) using STAR software (version 2.5.3a) with default parameters.²⁴ Then the distribution, coverage, homogeneity, and chain specificity of reads were evaluated by RSeQC (version 2.6).²⁵ Peaks in the ChIP-Seq datasets were called with MACS2 (version 2.1.1)²⁶ and associated with genes using Homer (version v4.10).^{26,27} The distribution of call peak on the chromosomes and functional elements was performed by deepTools (version 2.4.1)²⁸ and ChIPseeker (version 1.5.1).²⁹ Peak maps of reads across the genome are described using IGV (version 2.4.16).³⁰ The motif analysis was performed using Homer (version v4.10).²⁷ Gene ontology (GO) analysis and Kyoto encyclopedia of genes and genomes (KEGG) enrichment analysis for the peak related genes were both implemented by KOBAS software (version: 2.1.1) with a corrected P-value cutoff of 0.05 to judge statistically significant enrichment.³¹ Signal tracks of features (H3K9me2 and H3K9me3) were calculated by using DeepTools with parameter "ComputeMatrix." We remove the noise by subtracting the INPUT matrix from the IP matrix and showed the

features at peaks regions and up- and downstream regions within ± 2 kb.

2.9 | Digital RNA-seq

2.9.1 | RNA extraction, library preparation, and sequencing

Total RNAs were extracted from samples using TRIzol (Invitrogen) following the methods.³² DNA digestion was carried out after RNA extraction by DNase I. RNA quality was determined by examining A260/A280 with Nanodrop™ One spectrophotometer (Thermo Fisher Scientific Inc). RNA Integrity was confirmed by 1.5% agarose gel electrophoresis. Qualified RNAs were finally quantified by Qubit3.0 with Qubit™ RNA Broad Range Assay kit (Life Technologies).

A quantity of 2 μ g total RNAs were used for stranded RNA sequencing library preparation using KC-Digital™ Stranded mRNA Library Prep Kit for Illumina (Catalog NO. DR08502, Wuhan Seqhealth Co., Ltd. China) following the manufacturer's instruction. The kit eliminates duplication bias in PCR and sequencing steps, by using unique molecular identifier (UMI) of 8 random bases to label the pre-amplified cDNA molecules. The library products corresponding to 200-500 bps were enriched, quantified, and finally sequenced on Hiseq X 10 sequencer (Illumina).

2.9.2 | RNA-Seq data analysis

Raw sequencing data was first filtered by Trimmomatic (version 0.36),²³ low-quality reads were discarded and the reads contaminated with adaptor sequences were trimmed. Clean Reads were further treated with in-house scripts to eliminate duplication bias introduced in library preparation and sequencing. Briefly, clean reads were first clustered according to the UMI sequences, in which reads with the same UMI sequence were grouped into the same cluster, resulting in 65 536 clusters. Reads in the same cluster were compared to each other by pairwise alignment, and then reads with sequence identity over 95% were extracted to a new sub-cluster. After all sub-clusters were generated, multiple sequence alignment was performed to get one consensus sequence for each sub-cluster. After these steps, any errors and biases introduced by PCR amplification or sequencing were eliminated.^{33,34}

The de-duplicated consensus sequences were used for standard RNA-seq analysis. They were mapped to the reference genome of *Sus scrofa* from GCF_000003025.6 (ftp://ftp.ncbi.nlm.nih.gov/genomes/all/GCF/000/003/025/GCF_000003025.6_Sscrofa11.1/GCF_000003025.6_Sscrofa11.1_genomic.fna.gz) using STAR software (version 2.5.3a)²⁴ with

default parameters. Reads mapped to the exon regions of each gene were counted by feature Counts (Version 1.5.1)³⁵ and then FPKMs were calculated. Genes differentially expressed between groups were identified using the edgeR package (version 3.12.1).³⁶ An FDR corrected *P* value cutoff of .05 and fold-change cutoff of 2 were used to judge the statistical significance of gene expression differences. Gene ontology (GO) analysis and Kyoto encyclopedia of genes and genomes (KEGG) enrichment analysis for differentially expressed genes were both implemented by KOBAS software (version: 2.1.1) with a corrected *P* value cutoff of .05 to judge statistically significant enrichment.^{31,37,69-70} We clustered and showed our data through hierarchical clustering of R package “pheatmap” with parameter “cutree_rows” based on cluster results. Hierarchical clustering was performed with a distance matrix between two parts. Distance measure used in clustering rows by calculating Pearson correlation.

2.10 | ATAC-seq

5×10^4 cells were treated with cell lysis buffer and nucleus was collected by density gradient centrifuging for 30 minutes at 120 000g in 60% Percoll and 2.5 M sucrose solution. Transposition and high-throughput DNA sequencing library were carried out by TruePrep DNA Library Prep Kit V2 for Illumina kit (Catalog NO. TD501, Vazyme). The library was sequenced on Novaseq 6000 sequencer (Illumina).

Raw sequencing data were first filtered by Trimmomatic (version 0.36). Clean Reads were further treated with FastUniq (version 1.1) to eliminate duplication. Reads were mapped to the reference genome of *Sus scrofa* from GCF_000003025.6 using bowtie2 software (version 2.2.6) with default parameters. The MACS2 software (version 2.1.1) was used for peak calling, and the Homer (version 4.10) was used for motifs analysis. We got OS binding sites from ChIP-seq of O/S. Then, genome signal tracks matrix of ATAC-seq nearby O/S sites were calculated by computeMatrix of deeptools. Signal of ATAC-seq nearby O/S sites were visualized by ggplot2.

2.11 | IP-MS

2.11.1 | Immunoprecipitation

1×10^7 cells were digested by TrypLE Select and then transferred immediately to a 1.5-mL tube on ice. The cell suspension was then centrifuged at 5000g for 3 minutes and supernatant was discarded. The cell sediment was lysed by IP buffer (Beyotime, P0013) for 30 minutes on ice and then centrifuged at 12 000 g for 10 minutes and supernatant was collected. The supernatant was incubated with anti-FLAG magnetic beads (Sigma, F2426) overnight at 4°C, washed

five times with IP buffer, added to 5× SDS-PAGE loading buffer (GENSHARE G, JC-PE007), and heated at 100°C for 5 minutes. Immunoprecipitates were subjected to SDS-PAGE and probed with indicated antibodies.

2.11.2 | Mass spectrometry

In-gel digestion

For in-gel tryptic digestion, gel pieces were destained in 50 mM NH₄HCO₃ in 50% acetonitrile (v/v) until clear. Gel pieces were dehydrated with 100 μL of 100% acetonitrile for 5 minutes, the liquid was removed, and the gel pieces rehydrated in 10 mM dithiothreitol and incubated at 56°C for 60 minutes. Gel pieces were again dehydrated in 100% acetonitrile, the liquid was removed and gel pieces were rehydrated with 55 mM iodoacetamide. Samples were incubated at room temperature in the dark for 45 minutes. Gel pieces were washed with 50 mM NH₄HCO₃ and dehydrated with 100% acetonitrile. Gel pieces were rehydrated with 10 ng/μL trypsin resuspended in 50 mM NH₄HCO₃ on ice for 1 hour. Excess liquid was removed and gel pieces were digested with trypsin at 37°C overnight. Peptides were extracted with 50% acetonitrile/5% formic acid, followed by 100% acetonitrile. Peptides were dried to completion and resuspended in 2% acetonitrile/0.1% formic acid.

LC-MS/MS analysis

The tryptic peptides were dissolved in 0.1% formic acid (solvent A), directly loaded onto a home-made reversed-phase analytical column (15 cm length, 75 μm i.d.). The gradient was comprised of an increase from 6% to 23% solvent B (0.1% formic acid in 98% acetonitrile) over 16 minutes, 23% to 35% in 8 minutes and climbing to 80% in 3 minutes then holding at 80% for the last 3 minutes, all at a constant flow rate of 400 nL/min on an EASY-nLC 1000 UPLC system.

The peptides were subjected to NSI source followed by tandem mass spectrometry (MS/MS) in Q Exactive™ Plus (Thermo) coupled online to the UPLC. The electrospray voltage applied was 2.0 kV. The m/z scan range was 350–1800 for full scan, and intact peptides were detected in the Orbitrap at a resolution of 70 000. Peptides were then selected for MS/MS using NCE setting as 28 and the fragments were detected in the Orbitrap at a resolution of 17 500. A data-dependent procedure that alternated between one MS scan followed by 20 MS/MS scans with 15.0 seconds dynamic exclusion. Automatic gain control (AGC) was set at 5E4.

The resulting MS/MS data were processed using Proteome Discoverer 1.3. Tandem mass spectra were searched against UniPort database. Trypsin/P (or other enzymes if any) was specified as cleavage enzyme allowing up to two missing cleavages. The mass error was set to 10 ppm for precursor ions and 0.02 Da for-fragment ions. Carbamidomethyl on Cys were specified as fixed modification and oxidation on

Met was specified as variable modification. Peptide confidence was set at high, and peptide ion score was set >20.

2.12 | Luciferase assay for enhancer activity

All luciferase vectors were derived from PGL3-basic vector (Promega, E1751) by Seamless Cloning. Luciferase activity was measured using dual-luciferase detection kit (Beyotime, RG027) as described in the manufacturer's procedure.³⁸

2.13 | Statistical analysis

All the experiments had at least three independent biological replicates, except RNA-seq which were replicated twice. The ChIP samples were collected from three independent biological experiments, then mixed for ChIP-seq. Statistical significance was accepted at $P < .05$ and calculated using one-way ANOVA in Excel 2016.

3 | RESULTS

3.1 | H3K9 demethylation maintains the pluripotency of piPSCs

The piPSCs depended on the sustained expression of exogenous genes, which were similar to other reported piPSCs.^{21,39,40,41} The clonal morphology and pluripotency gradually disappeared after the piPSCs cultured in differentiation medium without doxycycline (DOX) and feeder (Figure 1A). The expression of both exogenous and endogenous pluripotent genes (*OCT4*, *SOX2*, *LIN28A*, and *NANOG*) were downregulated in this treatment (Figure 1B,C). Analysis of global histone methylation showed that the level of H3K9me1/2/3 was significantly increased (Figure 1C). Further analysis showed the expression of *KDM3A/3B/3C/4B/4C*, which are H3K9 demethylase, was downregulated significantly (Figure 1D). These results indicated that the H3K9 hypomethylation and pluripotent factors *OCT4* and *SOX2* were associated with maintaining the pluripotency of piPSCs. Additionally, the H3K9 demethylase *KDM3A/3B/3C/4B/4C* might be involved in this process of pluripotent maintenance.

To investigate the mechanism in detail, we screened a series of key components in the culture medium (Figure S1A). The results showed that the pluripotency of piPSCs mainly depends on two small molecule inhibitors (chir99021 and sb431542), DOX, and feeder (Figures 2A, S1A). Given that the expression of *KDM3A* was significantly downregulated during differentiation (Figure 1D), we further tested the expression of *KDM3A* in different treatments. The results

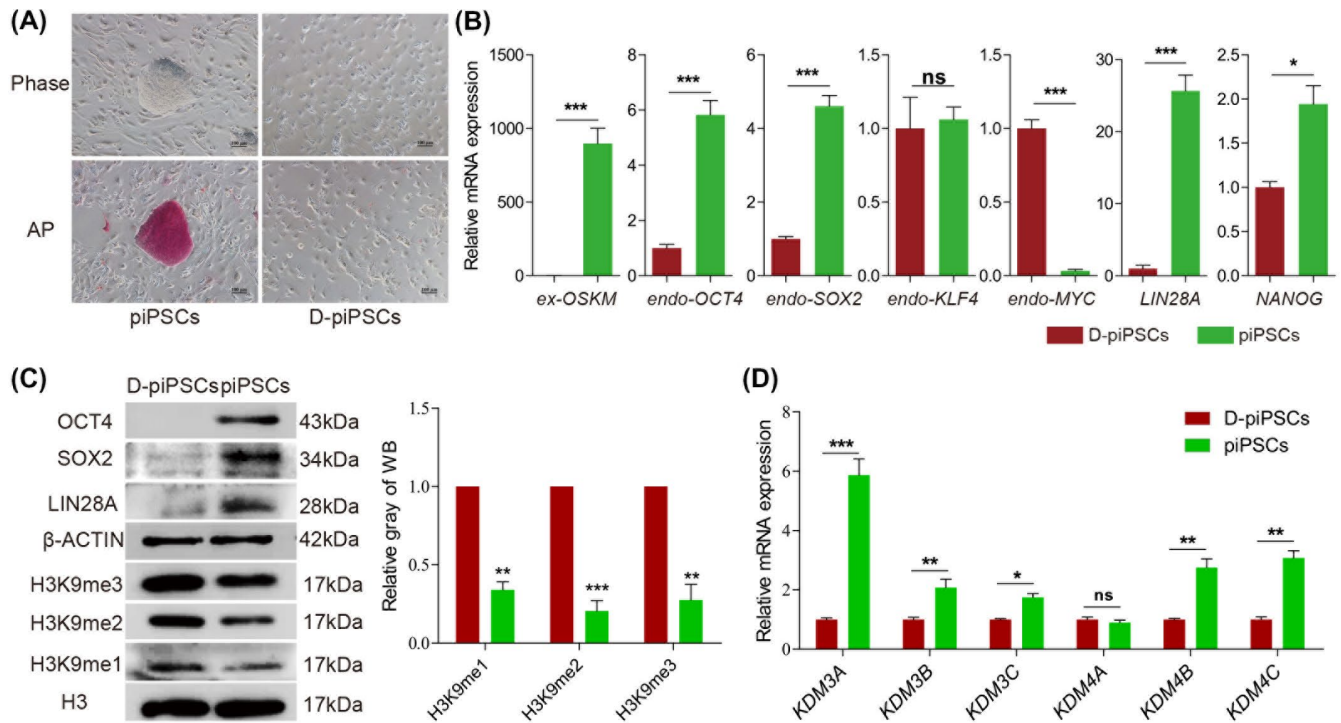


FIGURE 1 The loss of pluripotency was accompanied by the increase of H3K9 methylation and the decrease of corresponding demethylase. A, Representative image of AP staining of piPSCs and D-piPSCs (differentiated piPSCs). The D-piPSC represents piPSCs after 5 days of culture under differentiation medium. The experiments were performed at least three times. The scale bar represents 100 μ m. B, RT-qPCR analysis of the exogenous reprogramming factors and endogenous pluripotent genes in the piPSC and D-piPSC. The relative expression levels were normalized to β -actin. Data represent the mean \pm SD; n = 3 independent experiments. C, Representative Western-Blot of OCT4, SOX2, LIN28A, and H3K9me1/2/3 after 5 days of culture in the indicated conditions. The quantitative analysis of H3K9me1/2/3 is shown by bar graph. Data represent the mean \pm SD and was normalized by H3; n = 3 independent experiments. D, RT-qPCR analysis of *KDM3A/3B/3C* and *KDM4A/B/C* in the piPSC and D-piPSC. The relative expression levels were normalized to β -actin. Data represent the mean \pm SD; n = 3 independent experiments

showed that the expression of *KDM3A* was affected by feeder. Interestingly, the expression of *KDM3A* was not impeded when DOX was removed, but it was further downregulated when DOX was removed under F- treatment (Figure S1B). These results suggested the possible pivotal role of feeder and core pluripotent factors in reducing H3K9 methylation.

To explore the mechanisms of increased H3K9 methylation under the feeder-free condition, we focused on the effects of F- and FD- treatments. With the disappearance of typical clone morphology, lower proliferation rate, and high rate of apoptosis under both conditions were observed (Figures 2A, S2A-C). The expression levels of OCT4 and SOX2 were gradually downregulated, whereas those of KLF4 and c-MYC were significantly upregulated (Figure 2B,C). The expression of *LIN28A* increased significantly in F- treatment however decreased significantly in FD- treatment (Figure 2B,C). Immunofluorescence also confirmed that the total expressions of OCT4 and SOX2 were significantly decreased and that the piPSCs gradually differentiated into the ectoderm and mesoderm (Figure S2D,E). These results indicated the pluripotency of piPSCs gradually vanished under F- and FD-treatments. The loss of pluripotency gene expression prompts us to check repression related epigenetic modification H3K9

methylation in these cells. The results revealed that the expression of *KDM3A/3B/3C/4C* genes was remarkably decreased and H3K9 methylation was gradually increased in F- and FD- treatments (Figure 2C,D,F). Further immunofluorescence analysis demonstrated that the fluorescence intensity of H3K9me2/me3 at the marginal zone of clone was higher than that inside in the F- treatments (Figure 2E). This result was closely associated with the phenotype of cell marginal differentiation. These observations suggested that the increased H3K9me2/me3 in the F- and FD- treatments was significantly associated with differentiation.

3.2 | Feeder and pluripotent factors synergize to construct the pluripotency network

We attempted to gain insights into the molecular consequences that were triggered in response to the action of these treatments. RNA sequencing was performed to provide a snapshot of the transcriptional dynamics after the pluripotency changed. Transcriptional changes in both directions were observed in F- (272 up versus 443 down) and

FD- treatments (1786 up versus 1144 down; Figure 3A). Notably, downregulated genes accounted for the majority in the differentially expressed genes (DEGs) in F- treatment (Figure 3A). Given the significant increase of H3K9me2/3 in this treatment, feeders might promote the gene expression by facilitating the erasure of H3K9me2/3. However, more upregulated transcription was observed in FD- treatment (Figure 3A), suggesting that core pluripotent factors

mainly inhibited transcriptional output to maintain pluripotency. Further analysis showed 200 of 272 upregulated genes in the F- treatment were also upregulated in FD- treatment, and 226 of 443 downregulated genes in the F- treatment were also downregulated in FD- treatment (Figure 3B), indicating that these two treatments went through a consecutive process of differentiation. Additionally, the RNA-seq again demonstrated pluripotency-related genes and *KDM3A/3B/4C*

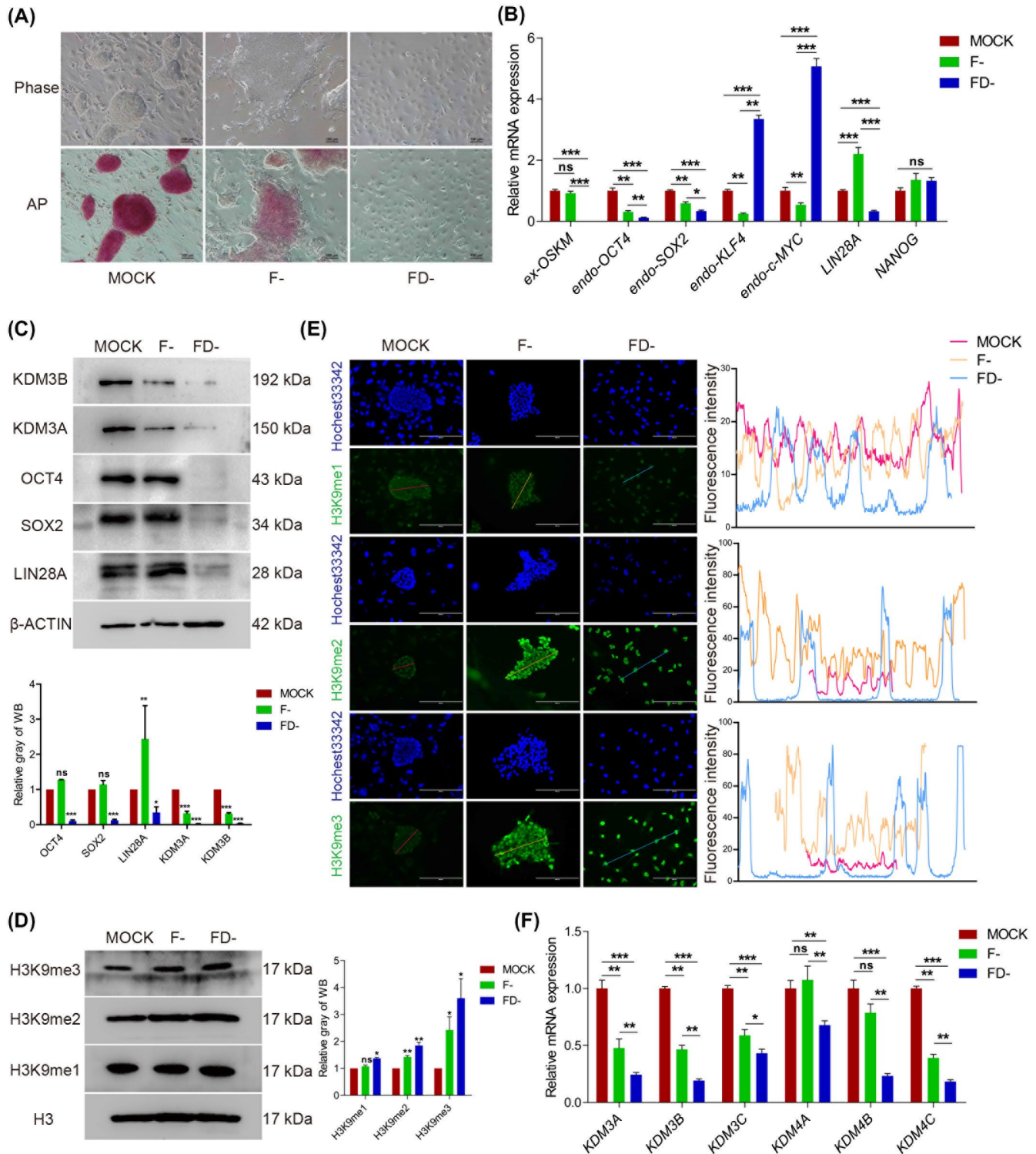


FIGURE 2 Feeder and exogenous genes affect the global H3K9 methylation in piPSCs. A, Representative image of Alkaline Phosphatase (AP) stained colonies after 5 days of clonal growth in the F- (feeder free) and FD- (feeder free and absence of Dox) treatments. The MOCK represents piPSCs grown under normal condition as a blank control. The experiments were performed three times. The scale bar represents 100 μm . B, RT-qPCR analysis of the exogenous reprogramming factors and endogenous pluripotent genes in the F- and FD- treatments. The relative expression levels were normalized to β -actin. Data represent the mean \pm SD; n = 3 independent experiments. C, Representative Western-Blot of OCT4, Sox2, LIN28A, KDM3A, and KDM3B after 5 days of culture in the indicated conditions. The quantitative analysis is shown by histogram. Data represent the mean \pm SD; n = 3 independent experiments. D, Representative Western-Blot of H3K9me1/2/3 after 5 days of culture in the indicated conditions. The quantitative analysis is shown by histogram. Data represent the mean \pm SD; n = 3 independent experiments. E, Immunofluorescence analysis of H3K9me1/2/3 in the indicated conditions. Intensity values along the indicated path were obtained using ImageJ and shown by line chart. The nuclei were DAPI stained. The scale bar represents 200 μm . The experiments were performed three times. F, RT-qPCR analysis of *KDM3A/3B/3C* and *KDM4A/4B/4C* in the F- and FD- treatments. The relative expression levels were normalized to β -actin. Data represent the mean \pm SD; n = 3 independent experiments

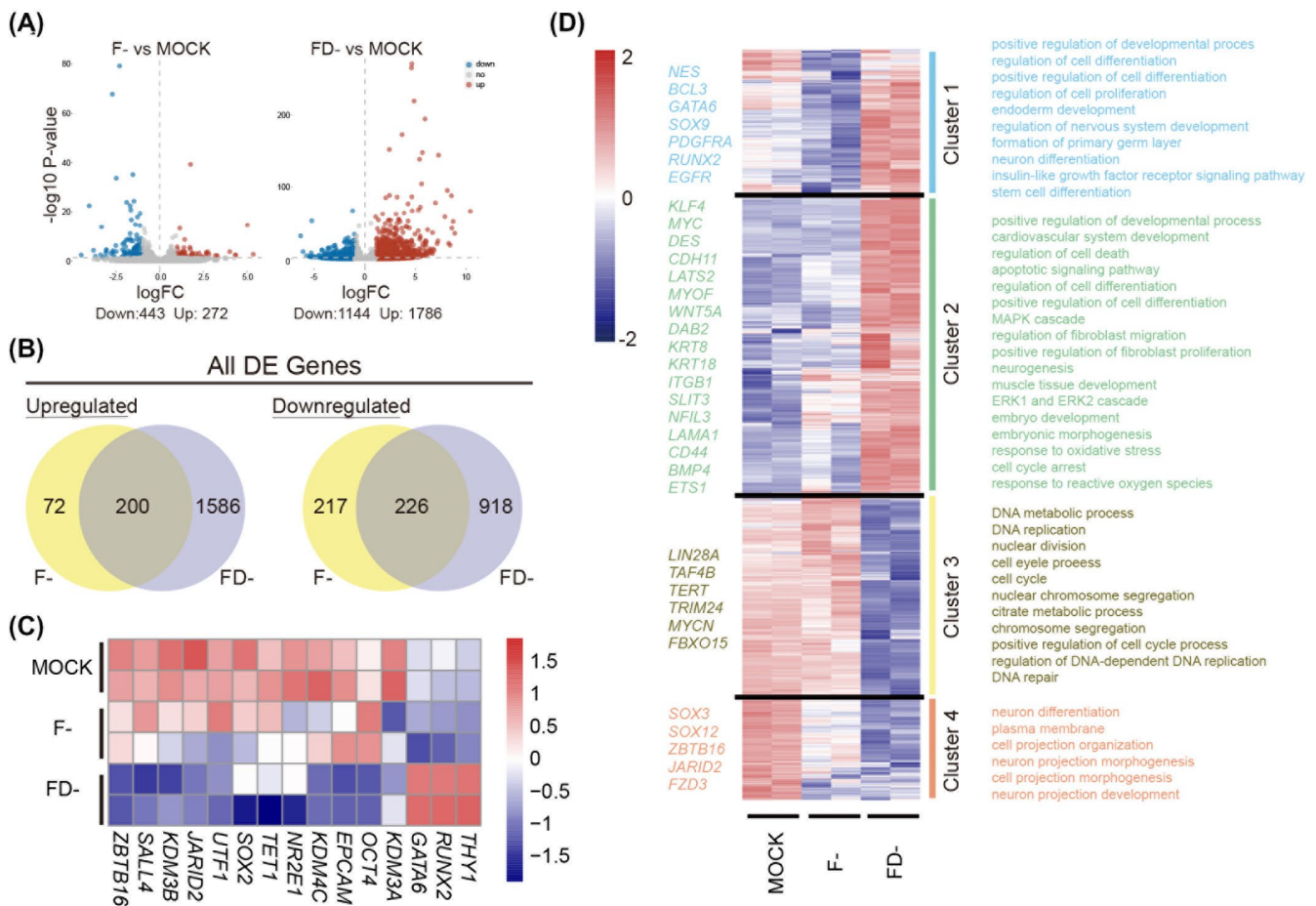


FIGURE 3 Feeder and exogenous genes cooperatively facilitate pluripotent transcriptional responses and inhibit the expression of differentiated related genes. A, The volcano plot showing the number of up- or downregulated differentially expressed (DE) genes between F- and FD- conditions on day 5 determined by RNA-Seq. n = 2 independent experiments. B, Venn diagrams showing the overlap of up- or downregulated differentially expressed (DE) transcripts between MOCK, F- and FD- conditions. C, Heat map (log10 scale and normalized by different treatment) showing changes in the expression of pluripotency, fibroblast markers, and epigenetic modification related genes in differentiating treatments obtained from RNA-Seq analysis. D, Four clusters of differential expression highlight the key differences between MOCK, F-, and FD- conditions. Gene ontology enrichment for each cluster is presented on the right. Represented genes of each cluster are listed on the left. Heatmap was processed with log10 scale and we also normalized FPKM with R package pheatmap by “scale (by different treatments)” function

showed a gradient descending tendency under F- and FD-treatments (Figure 3C). These results indicated that feeder and exogenous pluripotency genes processed a complementary regulation during piPSCs maintenance.

To further investigate this process, we applied cluster analysis for the DEGs. Gene ontology analysis of DEGs revealed significant enrichment in GO terms “positive regulation of developmental process,” “MAPK cascade,” “positive

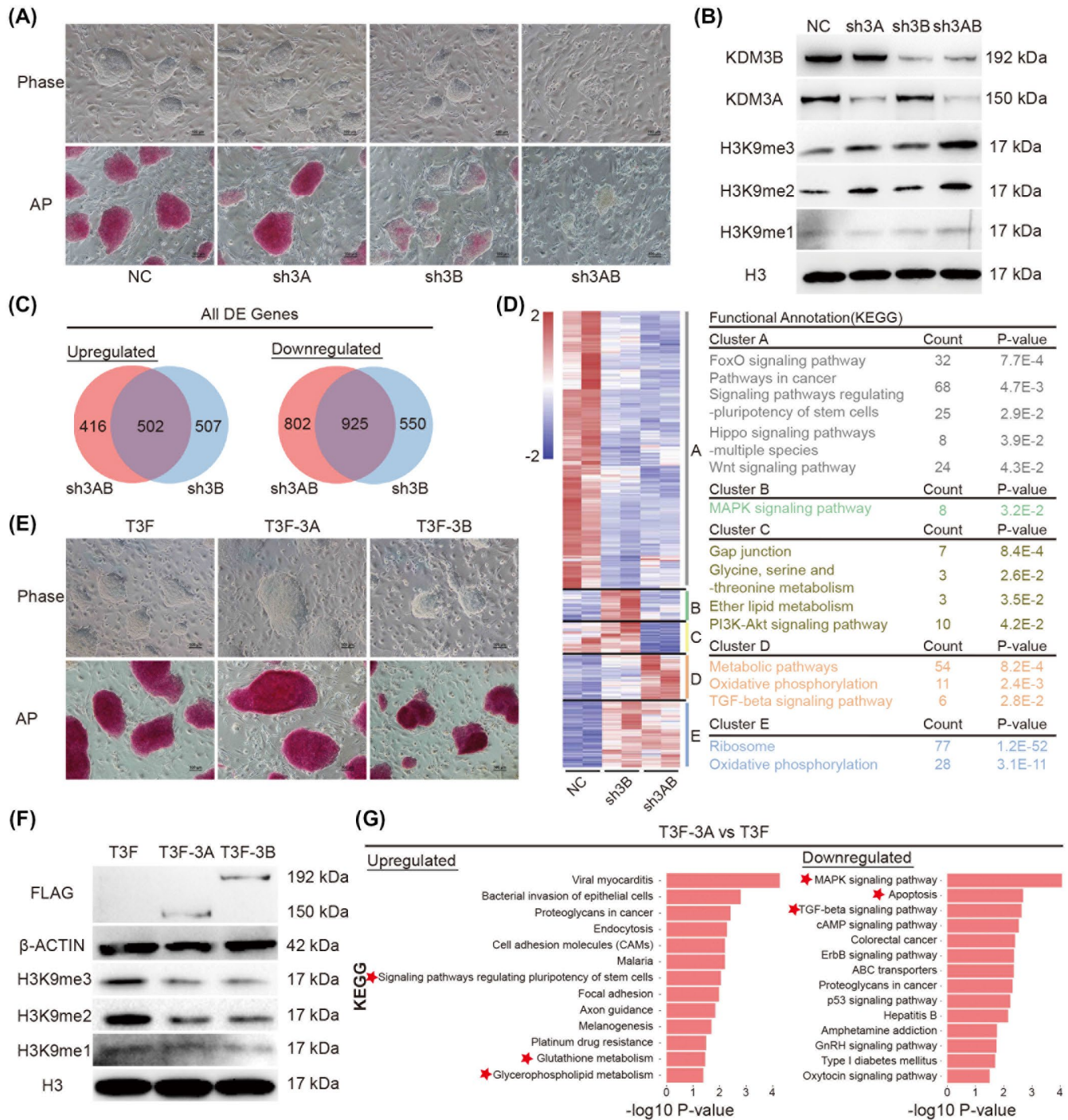


FIGURE 4 KDM3A and KDM3B synergize to maintain the pluripotency network in piPSCs. A, Representative image of AP-stained colonies after 5 days of clonal growth in the NC (Negative Control), sh3A(shKDM3A), sh3B(shKDM3B), and sh3AB (shKDM3A/B) cell lines. The experiments were performed three times. The scale bar represents 100 μ m. B, Representative Western-Blot of KDM3A, KDM3B, and H3K9me1/2/3 after 5 days of culture in the normal condition. n = 3 independent experiments. C, Venn diagrams showing the overlap of up- or downregulated differentially expressed (DE) transcripts between sh3B and sh3AB cell lines on day 5 determined by RNA-Seq. D, Five clusters of differential expression highlight the key differences between NC, sh3B, and sh3AB cell lines. Heatmap was processed with log₁₀ scale and we also normalized FPKM with R package pheatmap by “scale (by different treatments)” function. KEGG enrichment for each cluster is presented on the right. E, Representative image of AP-stained colonies after 5 days of clonal growth in the T3F (Empty vector), T3F-3A (overexpression of KDM3A) and T3F-3B (overexpression of KDM3A) cell lines. The experiments were performed three times. The scale bar represents 100 μ m. F, Representative Western-Blot of FLAG and H3K9me1/2/3 after 5 days of culture in the normal condition. The quantitative analysis of H3K9me1/2/3 is shown by bar graph in Figure S2F; n = 3 independent experiments. G, KEGG enrichment of up- or downregulated differentially expressed (DE) genes in T3F-3A cell lines

regulation of fibroblast proliferation,” and “cell cycle arrest” in response to F- and FD- treatments (Clusters 1 and 2; Figure 3D). FD- responsive downregulated genes were enriched for “neuronal differentiation,” “chromosome segregation,” and “DNA repair” (Clusters 3 and 4; Figure 3D). These results indicated the exogenous genes mainly inhibited the expression of differentiation-related genes and activated DNA repair-related genes to maintain the pluripotency of piPSCs. The cluster analysis also revealed that the feeder mainly promoted the expression of the SRY-related HMG-box (SOX) family of transcription factors (Clusters 1 and 4) to maintain the pluripotency of piPSCs which is consistent with feeder's function reported before.^{42,43} Some transcription factors in SOX family (Cluster 4) were co-activated by feeder and exogenous genes, such as *SOX3* (Figure 3D). The result suggested that epigenetic transcriptional activation mediated by feeder cooperated with pluripotent factors to drive the pluripotency gene regulatory network.

3.3 | Combined loss of KDM3A and KDM3B led to the collapse of the pluripotency network

To further directly investigate the role of H3K9 hypermethylation in the maintenance of piPSCs, the expressions of *KDM3A* and *KDM3B* were downregulated by shRNA. Unexpectedly, the depletion of *KDM3A* only resulted in a slight decrease in the proliferation of piPSCs (Figure S3A,B), and the global level of H3K9me2/3 was only slightly upregulated (Figure 4A,B). *KDM3B* loss not only significantly reduced the size of clones and proliferation rates, but also decreased the degree of AP staining. However, the level of H3K9me1/2/3 remained unchanged (Figure 4A,B). The results varied from previous studies on mESCs.^{6,7} *KDM3A* and *KDM3B* possess intrinsic H3K9 demethylating activity, so their functions may be complementary in the H3K9 demethylation. As expected, the co-depletion of *KDM3A* and *KDM3B* by shRNA induced a significant growth arrest and pluripotency loss in this group (Figures 4A,B, S3A,B). Consistent to this, H3K9me2/3 was increased significantly (Figure 4B). *KDM3B* could rescue the depletion of *KDM3A*, but *KDM3A* could not rescue that of *KDM3B*, suggesting that *KDM3B* might be involved in other biological processes.

To molecularly characterize *KDM3A/B* function, the profiles of the transcriptomes of shRNA treated samples (sh*KDM3A*, sh*KDM3B*, and sh*KDM3A/B* groups) were analyzed as well as empty vector control (NC) by RNA-sequencing. Although transcriptome did not change much in sh*KDM3A* group (11 up versus 27 down), the gene expression in sh*KDM3B* and sh*KDM3A/B* was observed significantly changing with 1099 and 918 upregulation; 1475 and 1727 downregulation respectively (Figure S3C). This finding

indicates the depletion of *KDM3A* alone had no significant effect on the pluripotency of piPSCs. Further analysis revealed sh*KDM3B* shared 50% (upregulated) and 63% (downregulated) dysregulated genes with sh*KDM3A/B* group, explaining why *KDM3B* could rescue the lack of *KDM3A* (Figure 4C).

The DEGs were then classified into five clusters (Figure 4D). KEGG analysis was performed on each cluster to clarify the effects of *KDM3A* and *KDM3B* on the maintenance of piPSCs. Genes with functions in pathways of “signaling pathways regulating pluripotency of stem cells,” “Wnt signaling pathway,” and “Pathways in cancer” were significantly downregulated in sh*KDM3B* and sh*KDM3A/B* groups (cluster A), whereas PI3K-Akt signaling pathway-associated genes were expressed at lower levels only in the sh*KDM3A/B* group (cluster C). The transcriptome analysis results suggested that the co-depletion of *KDM3A* and *KDM3B* destroyed the pluripotency of piPSCs by decreasing expression of genes related to “PI3K-Akt signaling pathway.” In addition, the piPSCs tended to differentiate and respond to oxidative stress, such as TGF-beta signaling pathway and oxidative phosphorylation, when depleted both *KDM3A* and *KDM3B* by shRNA (cluster D and E). These results suggested that erasure of H3K9me2/3 by *KDM3A* and *KDM3B* played a critical role in activating pluripotency related signaling pathways, such as PI3K-Akt signaling pathway.

3.4 | Histone demethylase KDM3A play a dominant role in maintaining pluripotency

Previous studies have demonstrated that the depletion of either *KDM3A* or *KDM3B* causes the increase of H3K9 methylation and loss of pluripotency in mESCs.^{6,7} However, a similar phenomenon only appeared in piPSCs when both *KDM3A* and *KDM3B* were downregulated, implying a novel and complex regulatory mechanism in piPSCs. To further reveal the demethylation mechanism regulated by *KDM3A/B*, they were respectively overexpressed in piPSCs (Figure 4E,F). The results showed that global H3K9me2/3 of piPSCs was remarkably decreased after overexpression of *KDM3A* or *KDM3B* (Figures 4F, S2F). Differences in clone phenotypes were observed between T3F-*KDM3A* and T3F-*KDM3B* groups (Figure 4E). Meanwhile, higher cell proliferation rate has been detected after *KDM3A* overexpression, while *KDM3B* overexpression inhibits cell proliferation (Figure S3D), suggesting that *KDM3A* and *KDM3B* were involved in different biological processes.

To analyze the molecular mechanism of *KDM3A* and *KDM3B* in piPSCs regulation, we profiled the transcriptomes of T3F-*KDM3A* and T3F-*KDM3B* by RNA-seq. We found *KDM3A* (460 up versus 283 down) and *KDM3B* (378 up versus 258 down) had divergent transcriptional output (Figure S3C). Only 128 upregulated genes and 76 downregulated overlapped

genes shared by the two groups, accounting for 18% and 16.4% of the total number of differently expressed genes, respectively (Figure S3E). The divergent transcriptional response again confirmed that KDM3A and KDM3B were involved in different biological processes. This finding explained why the depletion of KDM3B alone impairs the piPSCs pluripotency without altering global H3K9me2/3 modification. KEGG analysis was performed to clarify the effects of the overexpression of KDM3A and KDM3B on the maintenance of piPSCs. Genes with functions in pathways of “Signaling pathways regulating pluripotency of stem cells” were significantly upregulated in T3F-3A group, whereas genes associated with MAPK, apoptosis, and TGF-beta signaling pathways were downregulated only in T3F-3A group (Figure 4G). Nonetheless, overexpression of KDM3B enriched pathways unrelated to pluripotency (Figure S3F). We also found naive pluripotent gene *TBX3*^{44,45} and *WNT* ligands upregulated while the expression of *JUN* which inhibiting reprogramming downregulated after overexpression of KDM3A² (Figure S3G). However, the overexpression of KDM3B does not have the same effect. Together, our results suggested that the KDM3A maintained the pluripotent network of piPSCs by activating the expression of genes of signaling pathways regulating pluripotency as well as inhibiting genes associated with MAPK, apoptosis, and TGF-beta signaling pathways. The co-depletion of KDM3A and KDM3B influenced the pluripotency of piPSCs, but only overexpression of KDM3A could promote the pluripotency, suggesting KDM3A play a dominant role in maintaining pluripotency by H3K9 demethylation.

3.5 | H3K9me2/3 prevents pluripotent transcription factors regulating on the target genes

To further investigate the mechanism of KDM3A/B-mediated H3K9 demethylation on the maintenance of pluripotency, ChIP-seq of H3K9me2/3 was performed in MOCK and FD- groups. The result showed that the genome-wide level of H3K9me2/3 was significantly increased in FD- treatment (Figure 5A). The binding sites of H3K9me2/3 were located mainly in the intergenic region and intron rather than promoter, and no significant difference was noted between the MOCK and FD- near the transcription start sites (Figure S4A,B). These results suggested that H3K9me2/3 inhibited gene expression by acting on the other transcriptional regulatory regions other than promoters. To further clarify the role of H3K9me2/3 in the maintenance of pluripotent state, motif analysis of H3K9me2/3 peaks was performed. Results revealed that H3K9me2 peaks only bound sites in FD- group contained pluripotent transcription factor binding sites, such as OCT4 and SOX2 (Figure 5B). This result implied that H3K9me2 prevented interaction between pluripotent

transcription factors and their target genes. To confirm this, we found a significant enrichment of H3K9me2 modification occurred in the upstream enhancer region of pluripotent genes *OCT4* and *LIN28A* in the FD- group (Figure 5C), suggesting that these genes' expression was suppressed (Figures 2B, 3D). These results suggested that H3K9me2 represses gene expression by preventing the interaction between pluripotent transcription factors and target genes.

Combined analysis of ChIP-seq and RNA-seq of MOCK and FD- groups were performed to clarify the relationship between H3K9me2/3 and pluripotency maintenance. Considering that H3K9 methylation will silence gene expression, the associated genes were divided into four parts: the downregulated genes marked by FD- specified H3K9me2/3; the upregulated genes marked by MOCK specified H3K9me2/3. Further GO analysis of genes in Parts 1 and 3 reveal their enrichment in “positive regulation of fibroblast proliferation,” “positive regulation of apoptotic process,” “positive regulation of ERK1 and ERK2 cascade,” and “positive regulation of epithelial to mesenchymal transition” (Figure S4C). The genes in Parts 2 and 4 included several potential pluripotent genes, such as *NR6A1* (Figure S4C).⁴⁶ The result suggested that H3K9me2/3 participated not only in the inhibition of pluripotent genes during differentiation, but also in the inhibition of somatic genes in the pluripotent state.

3.6 | O/S and KDM3A/3B synergize to construct the porcine pluripotent networks

To further investigate how H3K9 demethylation occurs specifically in pluripotent gene regions, ChIP-seq of OCT4 and SOX2 were performed to anchoring the distribution of two core pluripotent transcription factors in genome. The results showed that the binding sites of OCT4 and SOX2 were also located in the intergenic region and intron rather than promoter (Figure S5A). It is noteworthy that the OCT4 shares about 50% (5554) peaks with SOX2, which accounts for 74.6% (3376/4523) of the genes OCT4 target (Figure S5B), supporting interaction between OCT4 and SOX2 during binding to maintain gene expression. These findings were similar to the results reported in mouse.^{1,47,48}

Given the dependence between transcription factors O/S and hypomethylation of H3K9 in this study (Figure 5B), the relationship between them might be a cooperators. To further explore the physiological relevance of our findings that OCT4 and SOX2 maintain piPSCs pluripotency is dependent on H3K9 hypomethylation, we explore how many OCT4 and SOX2 peaks co-occupied by H3K9me2/3. Finally, we found about 20% OCT4 (18%, 1984/10817) and SOX2 (22%, 2346/10870) peaks modified by H3K9me2 (Figure 6A). Furthermore, we analyzed the change of H3K9me2/3 in OCT4 and SOX2 binding sites. The results showed the level of H3K9me2 at the OCT4

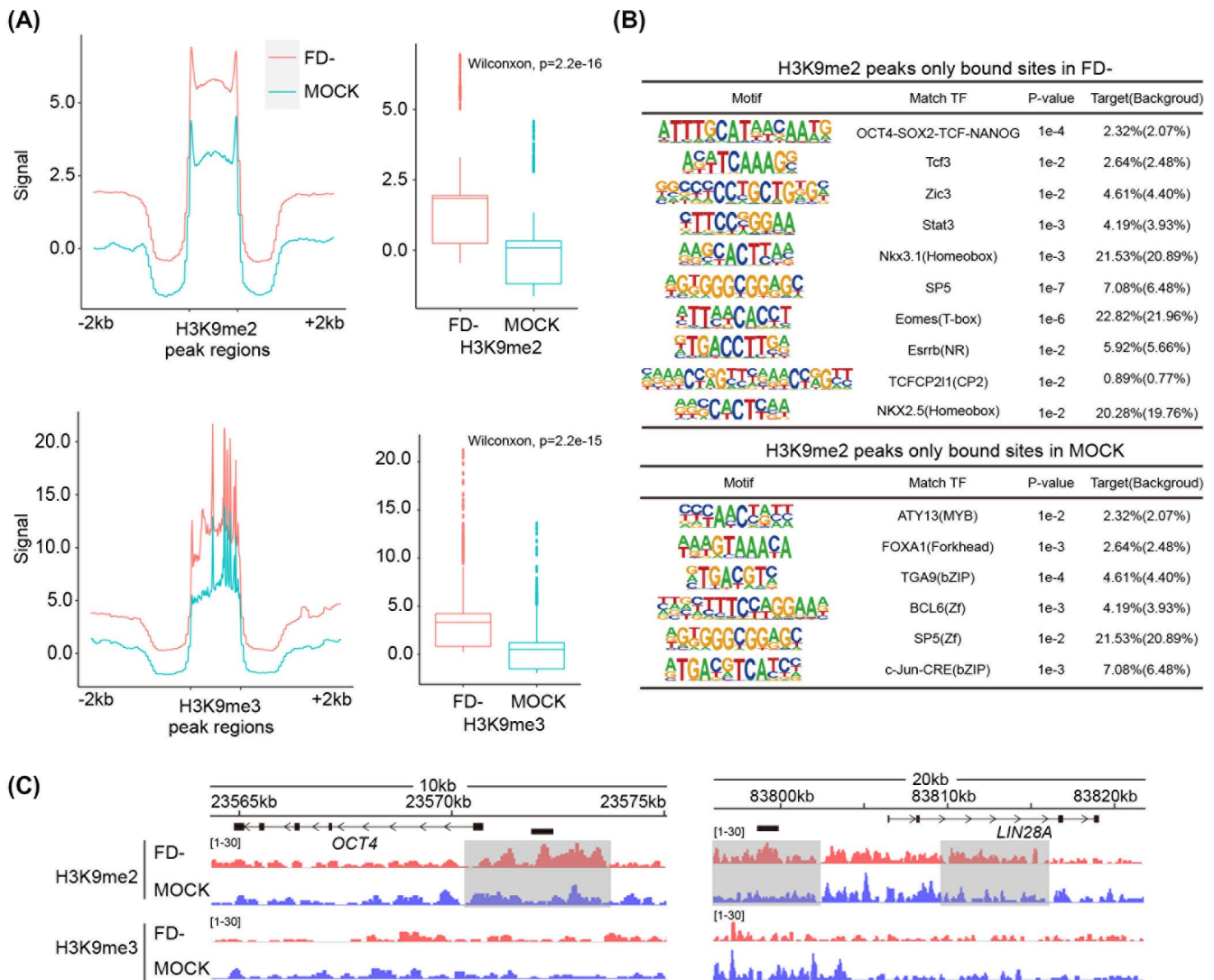


FIGURE 5 H3K9me2/3 prevents interaction between pluripotent transcription factors and target genes. A, Metaplots and boxplots of signal densities for H3K9me2/3 in MOCK and FD- treatments at all H3K9me2/3 bound sites. B, The motifs of H3K9me2 were identified at MOCK and FD- conditions. Last column: observed and expected motif frequencies (in parentheses). C, Chromatin immunoprecipitation-sequencing (ChIP-seq) analysis of H3K9me2/3 marks at pluripotency gene loci in MOCK and FD- conditions using IGV. Gray bars represent the H3K9 methylation difference area in MOCK and FD- conditions. The size of the peak represents the degree of enrichment

and SOX2 binding sites increased significantly in FD- group, indicating that H3K9 methylation directly prevented the function of OCT4/SOX2 (Figure 6B,C). The KEGG enrichment of peak-associated genes shared by OCT4/SOX2 and H3K9me2 showed that the genes were enriched in pathways like Wnt/ β -catenin signaling pathway which is important for pluripotency of stem cells regulation (Figure 6D). This result indicated that OCT4 and SOX2 drove critical pluripotent pathway depending on the erasure of H3K9me2. In addition, ATAC-seq of MOCK and FD- groups also showed that with the increase of H3K9me2 in the O/S binding sites, the accessibility of these sites in the FD-group decreased significantly (Figure 6E). ChIP-seq analysis further validates OCT4 and SOX2 binding to the enhancer and promoter regions of pluripotent genes *OCT4* and *LIN28A* in piPSCs, but these binding regions showed increased H3K9me2

in the FD- treatment, that is, the binding sites of OCT4 and SOX2 were closed (Figure 6F). These results suggested that OCT4 and SOX2 activated key pluripotent genes depending on the erasure of H3K9me2.

To further dissect the demethylation mechanism underlying KDM3A and KDM3B in the O/S binding sites, we applied IP-MS to directly investigate the proteins interacted to KDM3A and KDM3B under normal condition (Figures 7A,B, S5E). The results showed an interaction between KDM3A and KDM3B. Additional studies were conducted to verify the direct binding between KDM3A and KDM3B using a bimolecular fluorescence complementary (BiFC) technique (Figure S5E). GO analysis was performed on the proteins belonging to each part to clarify the different effects of KDM3A and KDM3B on the maintenance

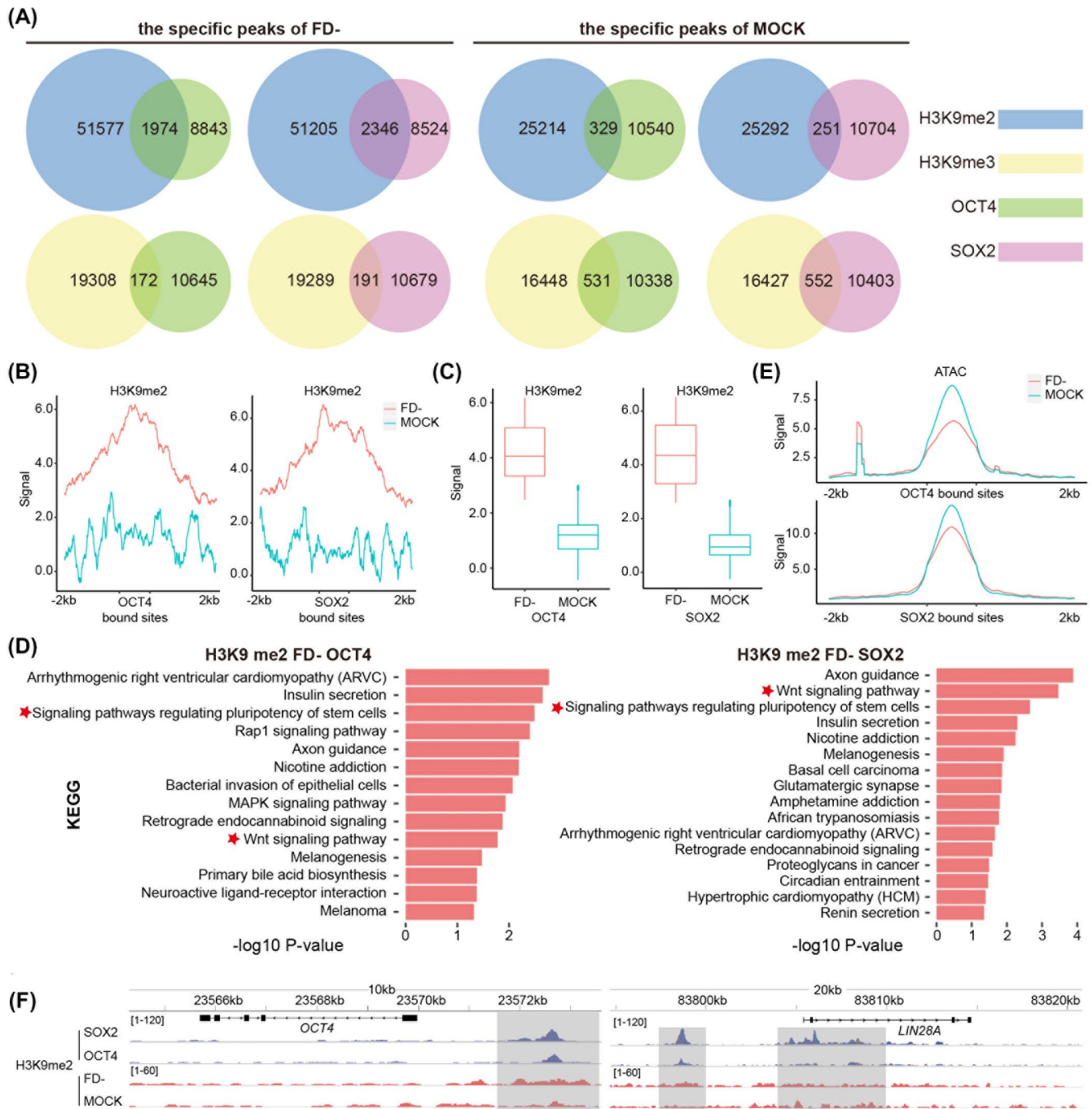


FIGURE 6 The demethylation of H3K9me2 is essential for O/S to activate pluripotent networks. **A**, Intersection of OCT4 or SOX2 binding sites and the specific H3K9me2/3 peaks of MOCK and FD-. The number of peaks for each part is given in the Venn diagram. Blue for H3K9me2 peaks, yellow for H3K9me3 peaks, green for oct4 peaks, and red for SOX2 peaks. **B**, Metaplots of signal densities for H3K9me2 in MOCK and FD- treatments at all OCT4 and SOX2 bound sites. **C**, Boxplots of H3K9me2 levels in MOCK and FD- treatments at all OCT4 and SOX2 bound sites. **D**, KEGG enrichment of the intersection of OCT4 or SOX2 binding sites and the specific H3K9me2 peaks in FD- associated gene. The red marks represent major pluripotent regulatory pathways. **E**, Metaplots of signal densities for ATAC-seq in MOCK and FD- treatments at all OCT4 and SOX2 bound sites. **F**, The chromatin immunoprecipitation-sequencing (ChIP-seq) analysis of OCT4 and SOX2 at pluripotency gene loci and H3K9me2/3 marks at pluripotency gene loci in MOCK and FD- conditions using IGV. The size of the peak represents the degree of enrichment

of piPSCs. Partners shared by KDM3A and KDM3B were enriched with functions in “DNA ligation involved in DNA repair,” “histone H3K9 demethylation,” and “DNA topological change.” KDM3A specific interacting proteins were

enriched with functions in “positive regulation of telomerase activity.” The specific KDM3B-interacting proteins were enriched with functions in “positive regulation of Wnt protein secretion” and “glycolytic process” (Figure 7C). These

results suggested that KDM3A and KDM3B co-regulated gene activation processes in the chromatin level but also individually involved in different biological processes. Further analysis of the IP-MS revealed that KDM3A interacted with SOX2, whereas KDM3B interacted with OCT4, which were further confirmed using IP-WB (Immunoprecipitation combined with western blot) (Figure 7B,D). A large number of high mobility group (HMG) proteins involved in chromatin remodeling^{49,50} were significantly enriched in the intersection of the IP-MS of KDM3A and KDM3B (Figure 7B). BiFC test again demonstrated the direct interaction between OCT4, SOX2, KDM3A, and KDM3B (Figure S5E). These results suggested that OCT4/SOX2, KDM3A/KDM3B, and HMG proteins formed a transcription complex to activate downstream genes. This new mechanism of pluripotency

maintenance is essential for the establishment of porcine naïve-state PSCs.

4 | DISCUSSION

The deconstruction of pluripotency gene regulatory network is a challenging and urgent issue need solving to obtain bona fide porcine pluripotent cells across the globe. In this study, we used the piPSCs generated by TetO-inducible system to gain a clear description of how the porcine epigenetic pluripotency network was maintained. Our results demonstrated that OCT4 and SOX2 cooperate with KDM3A/KDM3B to support the complex formation of super-transcription drivers to porcine pluripotency network.

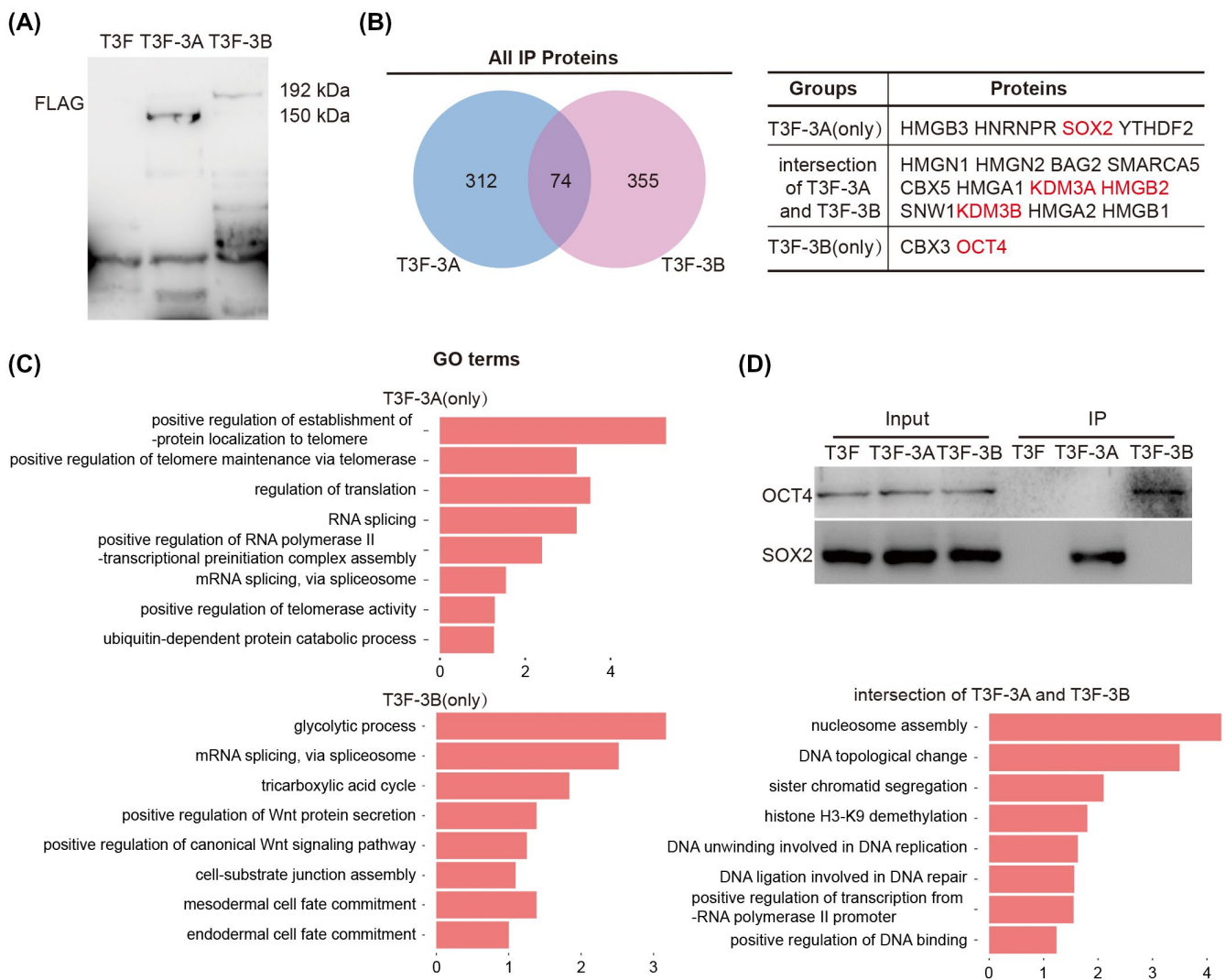


FIGURE 7 Cooperative binding of core transcription factors and KDM3A/B to maintain pluripotency. A, Immunoprecipitation of KDM3A and KDM3B were validated using western blot. piPSCs expressing 3×FLAG-KDM3A or 3×FLAG-KDM3B were used to purify KDM3A or KDM3B-associated proteins. The KDM3A or KDM3B-associated proteins were also detected and identified by mass spectrometry. B, Venn diagrams showing the overlap of KDM3A and KDM3B associated proteins determined by mass spectrometry. The table lists some representative proteins of each section. C, Gene ontology enrichment of KDM3A or KDM3B-associated proteins. D, The correlation between KDM3A, KDM3B, SOX2 and OCT4 were validated by western blotting

KDM3A/KDM3B-mediated H3K9 demethylation plays a critical role in early mouse embryogenesis and mES maintenance.⁶⁻⁸ However, no detailed information can be found on H3K9 methylation regulating porcine embryogenesis and ESC maintenance. In addition, the rules of KDM3A and KDM3B in H3K9 demethylation remained unclear. Our results demonstrated that KDM3A and KDM3B form a synergistic complex to perform demethylation, and only suppressing both of them will achieve global H3K9 hypermethylation. The conventional view is that KDM3A and KDM3B may function in a redundant manner.⁸⁻¹⁰ However, our study also suggests that KDM3A and KDM3B are novel cooperative mechanisms in the erasure of H3K9 methylation. The single-cell sequencing of porcine embryo shows that KDM3A is highly expressed in Morula, ICM, and Epiblast, but KDM3B is only specifically expressed in Epiblast (Figure S5D). The expression pattern was similar to SOX2, suggesting that a similar interaction mechanism might exist in Epiblast.⁵¹ Our results also reveal that the overexpression of KDM3A can significantly improve the proliferation and anti-apoptosis ability of pluripotent stem cells, but that of KDM3B leads to a decline in cell proliferation. The results suggest that KDM3A is the preferred choice for the H3K9 demethylation and excessive KDM3B affects pluripotency by promoting other biological processes under normal condition. Our study uncovers a novel mechanism in which histone demethylase performs H3K9 demethylation in porcine pluripotent stem cells.

Porcine pluripotent stem cells, including embryonic stem cells (ESCs) and iPSCs, are facing a very serious problem.⁵² At present, piPSCs can be obtained by ectopic expression of defined pluripotent transcription factors.^{41,53,54} However, the maintenance of pluripotent state depends on the continuous expression of exogenous genes, and endogenous pluripotent genes are not fully activated.^{39,40,41,53,54,55,56,57} Therefore, most of piPSCs also fail to contribute to chimeras with exceptions that are only detected by genomic PCR analysis.^{39,40} Porcine embryonic stem cell-like cells (pESLCs) exhibited some features of pluripotency, but these cells could not maintain self-renewal for a long time.⁵⁸⁻⁶¹ The generation of pESCs and acquisition of imperfect piPSCs always fail because the porcine endogenous pluripotent network cannot be maintained stably.

OCT4, which is a core factor during reprogramming, is often used as a marker for reprogramming cells to reach iPSC state.^{53,62,63} Numerous studies have shown that the depletion of OCT4 causes pluripotent stem cells to gradually lose their pluripotency.^{48,64} SOX2, a molecular marker specifically expressed in pig ICM,⁶⁵ cooperates with OCT4 to activate downstream pluripotent genes.^{47,48} According to our results, OCT4 and SOX2 together directly activate downstream target gene, and this finding is similar to that in other reports.^{1,47,48} Our study also demonstrates that the OCT4 and SOX2 are the core factors for the maintenance of piPSCs. Several studies on pig early embryos have indicated that OCT4 is generic expressed in ICM and TE, which differs from that in humans and mice (Figure S5D).⁵¹

The regulatory mechanism of endogenous OCT4 in pigs may be unique. Although our study did not further increase endogenous OCT4 by changing the culture system, we demonstrated that low expression of OCT4 is associated with high levels of H3K9me2 in its promoter and enhancer region (Figure 5C). We speculate that H3K9me2 level must be decreased in OCT4 promoter region during the establishment of porcine ESCs. LIN28A, as a downstream regulator of OCT4 and SOX2, was directly involved in the maintenance and metabolism of pluripotent stem cells, and influenced the transition between Naïve and Primed states.⁶⁶ In our study, we found OCT4 and SOX2 cooperatively binding to the upstream region of LIN28A, especially SOX2. In addition, the expression of LIN28A also decreased in FD- treatment, while its expression increased significantly in F-, indicating that it was also regulated by other factors. In previous study, OCT4 and LIN28A were also influenced by additional factors or chromatin conformation, such as H3K27ac or H3K4me.^{2,67,68} Our study demonstrated that both were inhibited by H3K9me2 during pluripotency maintenance in piPSCs. The erasure of H3K9me2 is necessary for the activation of both, rather than H3K9me3. However, the role of additional factors on both needs to be further investigated in piPSCs.

The IP-MS of KDM3A and KDM3B shows that both bind a large number of proteins associated with chromatin remodeling, such as HMGB2. Our further study demonstrates that SOX2 and OCT4 directly bind to KDM3A and KDM3B, respectively, suggesting that the SOX2/OCT4 recruit KDM3A/KDM3B and chromatin remodeling proteins form a transcriptional complex to drive the pluripotency gene regulatory network. This novel mechanism is similar to the previously reported super enhancer. Understanding the mechanistic basis for forming the complex between pluripotent and non-pluripotent cells reveals further insights into the nature of the pluripotent state.

ETHICS STATEMENT

All animal experiments were performed in strict accordance with the Guide for the Care and Use of Laboratory Animals (Ministry of Science and Technology of the People's Republic of China, Policy No. 2006398) and were approved by the Animal Care and Use Center of the Northwest A & F University.

ACKNOWLEDGMENTS

We thank Dr Yang Fan's helpful review and comments on the manuscript. We thank seqhealth technology co., LTD supplies technical support.

CONFLICT OF INTEREST

All authors read and approved the final manuscript and declare no competing financial interests.

AUTHOR CONTRIBUTIONS

Zhenshuo Zhu and Jinlian Hua designed the study and wrote the manuscript. Zhenshuo Zhu, Xiaolong Wu, Juqing Zhang,

Shuai Yu, Qiaoyan Shen, Zhe Zhou, Qin Pan, Wei Yue, Dezhe Qin, Ying Zhang, Wenxu Zhao, Rui Zhang performed the experiments. Zhenshuo Zhu, Qun Li, Sha Peng, Na Li, Shiqiang Zhang, Anmin Lei, Yiliang Miao, Zhonghua Liu, Huayan Wang, Mingzhi Liao, Jinlian Hua analyzed the data.

DATA AVAILABILITY STATEMENT

ChIP-seq and RNA-Seq data have been uploaded to National Center for Biotechnology Information Sequence Read Archive (SRA) database under the accession number PRJNA633419. The mass spectrometry proteomics data have been deposited to the ProteomeXchange Consortium (<http://proteomecentral.proteomexchange.org>) via the iProX partner repository⁶⁹ with the dataset identifier PXD016937.

ORCID

Zhenshuo Zhu  <https://orcid.org/0000-0003-0455-9509>
Jinlian Hua  <https://orcid.org/0000-0001-9788-8592>

REFERENCES

- Chronis C, Fiziev P, Papp B, et al. Cooperative binding of transcription factors orchestrates reprogramming. *Cell*. 2017;168(3):442-459 e420.
- Li D, Liu J, Yang X, et al. Chromatin accessibility dynamics during iPSC reprogramming. *Cell Stem Cell*. 2017;21(6):819-833 e816.
- Chen J, Liu HE, Liu J, et al. H3K9 methylation is a barrier during somatic cell reprogramming into iPSCs. *Nat Genet*. 2013;45(1):34-42.
- Sridharan R, Gonzales-Cope M, Chronis C, et al. Proteomic and genomic approaches reveal critical functions of H3K9 methylation and heterochromatin protein-1gamma in reprogramming to pluripotency. *Nat Cell Biol*. 2013;15(7):872-882.
- Tran KA, Jackson SA, Olufs ZPG, et al. Collaborative rewiring of the pluripotency network by chromatin and signalling modulating pathways. *Nat Commun*. 2015;6:6188.
- Loh YH, Zhang W, Chen X, George J, Ng HH. Jmjd1a and Jmjd2c histone H3 Lys 9 demethylases regulate self-renewal in embryonic stem cells. *Genes Dev*. 2007;21(20):2545-2557.
- Xiao F, Liao B, Hu J, et al. JMJD1C ensures mouse embryonic stem cell self-renewal and somatic cell reprogramming through controlling MicroRNA expression. *Stem Cell Reports*. 2017;9(3):927-942.
- Kuroki S, Nakai Y, Maeda R, et al. Combined loss of JMJD1A and JMJD1B reveals critical roles for H3K9 demethylation in the maintenance of embryonic stem cells and early embryogenesis. *Stem Cell Reports*. 2018;10(4):1340-1354.
- Kim J-Y, Kim K-B, Eom GH, et al. KDM3B is the H3K9 demethylase involved in transcriptional activation of lmo2 in leukemia. *Mol Cell Biol*. 2012;32(14):2917-2933.
- Yamane K, Toumazou C, Tsukada Y-I, et al. JHDM2A, a JmJc-containing H3K9 demethylase, facilitates transcription activation by androgen receptor. *Cell*. 2006;125(3):483-495.
- Wang H-Y, Long Q-Y, Tang S-B, et al. Histone demethylase KDM3A is required for enhancer activation of hippo target genes in colorectal cancer. *Nucleic Acids Res*. 2019;47(5):2349-2364.
- Li J, Yu B, Deng P, et al. KDM3 epigenetically controls tumorigenic potentials of human colorectal cancer stem cells through Wnt/beta-catenin signalling. *Nat Commun*. 2017;8:15146.
- Huang B, Wang B, Yuk-Wai Lee W, et al. KDM3A and KDM4C regulate mesenchymal stromal cell senescence and bone aging via condensin-mediated heterochromatin reorganization. *iScience*. 2019;21:375-390.
- Kuroki S, Matoba S, Akiyoshi M, et al. Epigenetic regulation of mouse sex determination by the histone demethylase Jmjd1a. *Science*. 2013;341(6150):1106-1109.
- Okada Y, Scott G, Ray MK, Mishina Y, Zhang Y. Histone demethylase JHDM2A is critical for Tnp1 and Prm1 transcription and spermatogenesis. *Nature*. 2007;450(7166):119-123.
- Liu Z, Zhou S, Liao L, Chen X, Meistrich M, Xu J. Jmjd1a demethylase-regulated histone modification is essential for cAMP-response element modulator-regulated gene expression and spermatogenesis. *J Biol Chem*. 2010;285(4):2758-2770.
- Saraç H, Morova T, Pires E, et al. Systematic characterization of chromatin modifying enzymes identifies KDM3B as a critical regulator in castration resistant prostate cancer. *Oncogene*. 2020;39(10):2187-2201.
- Liu Z, Chen X, Zhou S, Liao L, Jiang R, Xu J. The histone H3K9 demethylase Kdm3b is required for somatic growth and female reproductive function. *Int J Biol Sci*. 2015;11(5):494-507.
- Prather RS. Pig genomics for biomedicine. *Nat Biotechnol*. 2013;31(2):122-124.
- Walters EM, Prather RS. Advancing swine models for human health and diseases. *Mo Med*. 2013;110(3):212-215.
- Ma Y, Yu T, Cai Y, Wang H. Preserving self-renewal of porcine pluripotent stem cells in serum-free 3i culture condition and independent of LIF and b-FGF cytokines. *Cell Death Discov*. 2018;4:21.
- Zhu Z, Pan Q, Zhao W, et al. BCL2 enhances survival of porcine pluripotent stem cells through promoting FGFR2. *Cell Prolif*. 2021;54(1):e12932.
- Bolger AM, Lohse M, Usadel B. Trimmomatic: a flexible trimmer for Illumina sequence data. *Bioinformatics*. 2014;30(15):2114-2120.
- Dobin A, Davis CA, Schlesinger F, et al. STAR: ultrafast universal RNA-seq aligner. *Bioinformatics*. 2013;29(1):15-21.
- Wang L, Wang S, Li W. RSeQC: quality control of RNA-seq experiments. *Bioinformatics*. 2012;28(16):2184-2185.
- Zhang Y, Liu T, Meyer CA, et al. Model-based analysis of ChIP-Seq (MACS). *Genome Biol*. 2008;9(9):R137.
- Heinz S, Benner C, Spann N, et al. Simple combinations of lineage-determining transcription factors prime cis-regulatory elements required for macrophage and B cell identities. *Mol Cell*. 2010;38(4):576-589.
- Ramírez F, Ryan DP, Grüning B, et al. deepTools2: a next generation web server for deep-sequencing data analysis. *Nucleic Acids Res*. 2016;44(W1):W160-165.
- Yu G, Wang LG, He QY. ChIPseeker: an R/Bioconductor package for ChIP peak annotation, comparison and visualization. *Bioinformatics*. 2015;31(14):2382-2383.
- Thorvaldsdottir H, Robinson JT, Mesirov JP. Integrative Genomics Viewer (IGV): high-performance genomics data visualization and exploration. *Brief Bioinform*. 2013;14(2):178-192.
- Wu J, Mao X, Cai T, Luo J, Wei L. KOBAS server: a web-based platform for automated annotation and pathway identification. *Nucl Acids Res*. 2006;34(Web Server):W720-W724.
- Chomczynski P, Sacchi N. Single-step method of RNA isolation by acid guanidinium thiocyanate-phenol-chloroform extraction. *Anal Biochem*. 1987;162(1):156-159.
- Shugay M, Britanova OV, Merzlyak EM, et al. Towards error-free profiling of immune repertoires. *Nat Methods*. 2014;11(6):653-655.

34. Ma K-Y, He C, Wendel BS, et al. Immune repertoire sequencing using molecular identifiers enables accurate clonality discovery and clone size quantification. *Front Immunol.* 2018;9:33.
35. Liao Y, Smyth GK, Shi W. featureCounts: an efficient general purpose program for assigning sequence reads to genomic features. *Bioinformatics.* 2014;30(7):923-930.
36. Robinson MD, McCarthy DJ, Smyth GK. edgeR: a Bioconductor package for differential expression analysis of digital gene expression data. *Bioinformatics.* 2010;26(1):139-140.
37. Li N, Ma W, Shen Q, et al. Reconstitution of male germline cell specification from mouse embryonic stem cells using defined factors in vitro. *Cell Death Differ.* 2019;26(10):2115-2124.
38. Wei YD, Du XM, Yang DH, et al. Dmrt1 regulates the immune response by repressing the TLR4 signaling pathway in goat male germline stem cells. *Zool Res.* 2021;42(1):14-27.
39. Liu K, Mao J, Song L, et al. DNA repair and replication links to pluripotency and differentiation capacity of pig iPS cells. *PLoS One.* 2017;12(3):e0173047.
40. West FD, Terlouw SL, Kwon DJ, et al. Porcine induced pluripotent stem cells produce chimeric offspring. *Stem Cells Dev.* 2010;19(8):1211-1220.
41. Wu Z, Chen J, Ren J, et al. Generation of pig induced pluripotent stem cells with a drug-inducible system. *J Mol Cell Biol.* 2009;1(1):46-54.
42. Abdelalim EM, Emara MM, Kolatkar PR. The SOX transcription factors as key players in pluripotent stem cells. *Stem Cells Dev.* 2014;23(22):2687-2699.
43. Veerapandian V, Ackermann JO, Srivastava Y, et al. Directed evolution of reprogramming factors by cell selection and sequencing. *Stem Cell Reports.* 2018;11(2):593-606.
44. Wang J, Gu Q, Hao J, et al. Tbx3 and Nr5alpha2 play important roles in pig pluripotent stem cells. *Stem Cell Rev Rep.* 2013;9(5):700-708.
45. Han J, Yuan P, Yang H, et al. Tbx3 improves the germline competency of induced pluripotent stem cells. *Nature.* 2010;463(7284):1096-1100.
46. Hou D-R, Jin Y, Nie X-W, et al. Derivation of porcine embryonic stem-like cells from in vitro-produced blastocyst-stage embryos. *Sci Rep.* 2016;6:25838.
47. Narayan S, Bryant G, Shah S, Berrozpe G, Ptashne M. OCT4 and SOX2 work as transcriptional activators in reprogramming human fibroblasts. *Cell Rep.* 2017;20(7):1585-1596.
48. Malik V, Glaser LV, Zimmer D, et al. Pluripotency reprogramming by competent and incompetent POU factors uncovers temporal dependency for Oct4 and Sox2. *Nat Commun.* 2019;10(1):3477.
49. Hock R, Furusawa T, Ueda T, Bustin M. HMG chromosomal proteins in development and disease. *Trends Cell Biol.* 2007;17(2):72-79.
50. Zhu N, Hansen U. HMGN1 modulates estrogen-mediated transcriptional activation through interactions with specific DNA-binding transcription factors. *Mol Cell Biol.* 2007;27(24):8859-8873.
51. Ramos-Ibeas P, Sang F, Zhu Q, et al. Pluripotency and X chromosome dynamics revealed in pig pre-gastrulating embryos by single cell analysis. *Nat Commun.* 2019;10(1):500.
52. Ezashi T, Yuan Y, Roberts RM. Pluripotent stem cells from domesticated mammals. *Annu Rev Anim Biosci.* 2016;4:223-253.
53. Ezashi T, Telugu BP, Alexenko AP, Sachdev S, Sinha S, Roberts RM. Derivation of induced pluripotent stem cells from pig somatic cells. *Proc Natl Acad Sci U S A.* 2009;106(27):10993-10998.
54. Esteban MA, Xu J, Yang J, et al. Generation of induced pluripotent stem cell lines from Tibetan miniature pig. *J Biol Chem.* 2009;284(26):17634-17640.
55. Fujishiro S-H, Nakano K, Mizukami Y, et al. Generation of naive-like porcine-induced pluripotent stem cells capable of contributing to embryonic and fetal development. *Stem Cells Dev.* 2013;22(3):473-482.
56. Choi K-H, Park J-K, Son D, et al. Reactivation of endogenous genes and epigenetic remodeling are barriers for generating transgene-free induced pluripotent stem cells in pig. *PLoS One.* 2016;11(6):e0158046.
57. Mao J, Zhang Q, Deng W, et al. Epigenetic modifiers facilitate induction and pluripotency of porcine iPSCs. *Stem Cell Reports.* 2017;8(1):11-20.
58. Haraguchi S, Kikuchi K, Nakai M, Tokunaga T. Establishment of self-renewing porcine embryonic stem cell-like cells by signal inhibition. *J Reprod Dev.* 2012;58(6):707-716.
59. Cha H-J, Yun JI, Han NR, et al. Generation of embryonic stem-like cells from in vivo-derived porcine blastocysts at a low concentration of basic fibroblast growth factor. *Reprod Domest Anim.* 2018;53(1):176-185.
60. Kim S, Kim JH, Lee E, et al. Establishment and characterization of embryonic stem-like cells from porcine somatic cell nuclear transfer blastocysts. *Zygote.* 2010;18(2):93-101.
61. Xue B, Li Y, He Y, et al. Porcine Pluripotent Stem Cells Derived from IVF embryos contribute to chimeric development in vivo. *PLoS One.* 2016;11(3):e0151737.
62. Takahashi K, Yamanaka S. Induction of pluripotent stem cells from mouse embryonic and adult fibroblast cultures by defined factors. *Cell.* 2006;126(4):663-676.
63. Choi H, Joo J, Hong Y, et al. Distinct enhancer activity of Oct4 in naive and primed mouse pluripotency. *Stem Cell Reports.* 2016;7(5):911-926.
64. Chew J-L, Loh Y-H, Zhang W, et al. Reciprocal transcriptional regulation of Pou5f1 and Sox2 via the Oct4/Sox2 complex in embryonic stem cells. *Mol Cell Biol.* 2005;25(14):6031-6046.
65. Liu S, Bou G, Sun R, et al. Sox2 is the faithful marker for pluripotency in pig: evidence from embryonic studies. *Dev Dyn.* 2015;244(4):619-627.
66. Zhang J, Ratanasirintrao S, Chandrasekaran S, et al. LIN28 regulates stem cell metabolism and conversion to primed pluripotency. *Cell Stem Cell.* 2016;19(1):66-80.
67. Criqui M, Qamra A, Chu TW, et al. Telomere dysfunction cooperates with epigenetic alterations to impair murine embryonic stem cell fate commitment. *Elife.* 2020;9:e47333.
68. Fang L, Zhang J, Zhang H, et al. H3K4 methyltransferase Set1a is a key Oct4 coactivator essential for generation of Oct4 positive inner cell mass. *Stem Cells.* 2016;34(3):565-580.
69. Ma J, Chen T, Wu S, et al. iProX: an integrated proteome resource. *Nucleic Acids Res.* 2019;47(D1):D1211-D1217.

SUPPORTING INFORMATION

Additional Supporting Information may be found online in the Supporting Information section.

How to cite this article: Zhu Z, Wu X, Li Q, et al. Histone demethylase complexes KDM3A and KDM3B cooperate with OCT4/SOX2 to define a pluripotency gene regulatory network. *The FASEB Journal.* 2021;35:e21664. <https://doi.org/10.1096/fj.202100230R>